TOPICAL REVIEW — Low-dimensional nanostructures and devices

Metallic nanowires for subwavelength waveguiding and nanophotonic devices*

Pan Deng(潘 登), Wei Hong(魏 红), and Xu Hong-Xing(徐红星)†

Beijing National Laboratory for Condensed Matter Physics and Institute of Physics, Chinese Academy of Sciences, Beijing 100190, *China*

(Received 12 August 2013)

Plasmonics is a rapidly developing field concerning light manipulation at the nanoscale with many potential applications, of which plasmonic circuits are promising for future information technology. Plasmonic waveguides are fundamental elements for constructing plasmonic integrated circuits. Among the proposed different plasmonic waveguides, metallic nanowires have drawn much attention due to the highly confined electromagnetic waves and relatively low propagation loss. Here we review the recent research progress in the waveguiding characteristics of metallic nanowires and nanowire-based nanophotonic devices. Plasmon modes of both cylindrical and pentagonal metallic nanowires with and without substrate are discussed. Typical methods for exciting and detecting the plasmons in metallic nanowires are briefly summarized. Because of the multimode characteristic, the plasmon propagation and emission in the nanowire have many unique properties, benefiting the design of plasmonic devices. A few nanowire-based devices are highlighted, including quarter-wave plate, Fabry–Pérot resonator, router and logic gates.

Keywords: surface plasmons, waveguide, circuit, nanowire

PACS: 73.20.Mf, 42.79.Gn, 68.65.–k, 78.67.Uh **DOI:** 10.1088/1674-1056/22/9/097305

1. Introduction

The electronics-based integrated circuits have experienced rapid and exciting developments during the past decades, which are shown by famous Moore's Law. However, the development speed seems to begin to slow down and deviate from the Moore's Law recently, showing the limitation of electron as information carrier. This limitation, termed electron bottleneck, can be broken in all optical circuits and communication systems. The high velocity of photons indicates a giant enhancement of communicating speed to break the bottleneck limitation in electron based system. The photon has a wide communicating bandwidth which can benefit parallel computing. In recent years, quantum computing using photons has also been studied widely and shows application potential.[1]

Photonic integrated circuits have been developed based on large scale dielectric fibers and waveguides, and used for communication. However, because of the diffraction limit, light cannot be confined well below the scale of its wavelength, which limits the miniaturization of photonic circuits. The subwavelength confinement and waveguiding of light are vital for achieving highly compact on-chip optical circuits, which can be realized by resorting to surface plasmons, collective oscillations of free electrons in metal at the metal-dielectric interface. The researches related to surface plasmons have formed a new field called plasmonics, which covers a wide range of topics based on localized or propagating surface plasmons. In coupled metallic nanoparticles, localized surface plasmon resonances result in strong enhancement of electromagnetic field in the nanogaps,[2,3] which leads to many new phenomena and applications. In plasmonic waveguide structures, surface plasmon polaritons (SPPs) propagate at the interface of metal and dielectric with the electromagnetic field decaying sharply in exponential form on both sides of the interface, enabling the subwavelength confinement of propagating light. The basic structures for supporting the propagating surface plasmons are single metal-dielectric interface, metal–insulator–metal (MIM) structure and insulator–metal–insulator (IMI) structure.[4] These three kinds of two-dimensional (2D) structures have been demonstrated for subwavelength waveguiding and are usually used for interpreting subwavelength photonic devices in principle.

Besides the 2D waveguides, many more practical and complicated surface plasmon waveguides have been proposed theoretically based on computer simulations and realized experimentally due to the development of microfabrication techniques, such as dielectric loaded plasmonic waveguide,[5,6] slot[7] or V-groove[8,9] in metal film, metal wedge,[10,11] and metallic nanowire.[12] For all these waveguides, a basic trade-off between confinement and loss exists, which means that high confinement must be concomitant with high propagation loss. Metallic nanowire is much attractive since its supported

*Project supported by the National Basic Research Program of China (Grant No. 2009CB930700), the National Natural Science Foundation of China (Grant Nos. 11134013, 11227407 and 11004237), and the Knowledge Innovation Project of Chinese Academy of Sciences (Grant No. KJCX2-EW-W04).

†Corresponding author. E-mail: hxxu@iphy.ac.cn

plasmon modes have both considerable confinement and propagation length. All other plasmonic waveguides must utilize the top-down microfabrication techniques, which can induce nonideal rough surfaces and large additional scattering losses. Metallic nanowires can be fabricated using bottom-up chemical synthesis methods,[13] which produce nanowires of crystalline structure. Therefore, these wires have smooth surface and suffer low scattering loss.

In this review, we discuss the metallic nanowire plasmonic waveguide from its basic supported plasmon modes and waveguiding characteristics, to the nanowire-based photonic devices reported in the recent literature. The rest of this paper is arranged as follows. In Section 2, we discuss the plasmon modes of both cylindrical and pentagonal metallic nanowires. In Section 3, different methods of exciting plasmons in nanowire are presented. In Section 4, the typical methods to image the SPPs on nanowire are summarized. In Sections 5 and 6, the propagation and emission characteristics of the SPPs in nanowire are discussed based on the modes, respectively. In Section 7, some metallic-nanowire-based photonic devices are highlighted. Finally, some conclusions and tentative outlook are presented in Section 8.

2. Plasmon modes in silver nanowire

2.1. Eigenmodes of cylindrical nanowire

The surface plasmon polariton is a kind of propagating electromagnetic surface wave confined at metal–dielectric interface. The effective refractive index of the SPP wave is higher than the refractive index of the environment, enabling the confinement of electromagnetic energy during propagation. For an infinitely long metallic nanowire of cylindrical shape embedded in homogeneous dielectric environment, surface plasmon wave is confined near the surface of metallic nanowire and propagates along the z direction (Fig. 1(a)). The electromagnetic wave exists as evanescent wave both inside and outside the nanowire, similar to the SPPs at the metal–dielectric interface. The field distributions of the eigenmodes supported by the nanowire can be expressed as[14–16]

$$E_m(r,\phi,z) = A_m R_m(k_\perp r)\, \mathrm{e}^{\mathrm{i}m\phi}\, \mathrm{e}^{\mathrm{i}k_\parallel z}, \tag{1}$$

where $k_\parallel$ is the propagating wave vector along the nanowire; $k_\perp$ is the wave vector vertical to the nanowire, describing the decay of the field outside the nanowire; A_m is the amplitude of the m-order mode; R_m is the radial distribution in the form of m-order modified Bessel function of first or second kind in the metal and dielectric region, respectively; m is the index denoting the order of the eigenmodes; $\mathrm{e}^{\mathrm{i}m\phi}$ describes the angular distribution (ϕ is angular coordinate under cylindrical system). The m-order eigenmodes are doubly degenerated ($m > 0$). The fields of two m-order modes ($m > 0$) can be expressed as recombined forms to have $\sin(\phi)$ or $\cos(\phi)$ angular distributions. These modes can be named by following the ordinary rule for the modes in traditional dielectric cylindrical fiber.[17] The difference from dielectric fiber here is that only TM and HE mode can be supported in metallic nanowire.

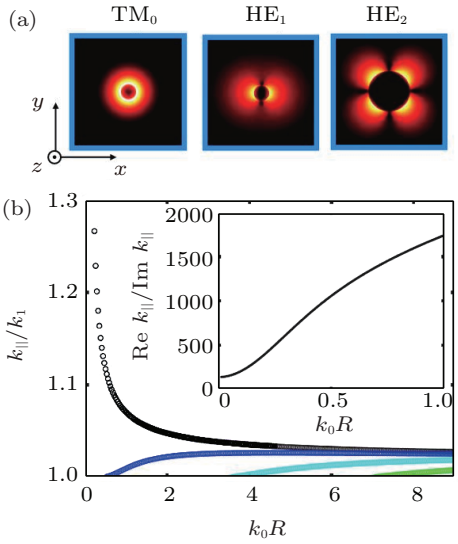

Fig. 1. (a) Field distributions and (b) dispersion relations of plasmon modes in silver nanowire in inhomogeneous dielectric environment with permittivity $\varepsilon = 2$. In panel (b), the black curve corresponds to fundamental TM_0 mode, and the others correspond to HE_m ($m = 1, 2, 3$) modes from left to right, respectively. The inset shows propagation loss for TM_0 mode characterized by $\mathrm{Re}(k_\parallel)/\mathrm{Im}(k_\parallel)$.[15,16]

The field distributions of three lowest order eigenmodes in nanowire are shown in Fig. 1(a). The lowest $m = 0$ mode is transverse-magnetic (TM) polarized, which means that the mode has no magnetic field parallel to the nanowire. The TM_0 mode is axially symmetric, and the direction of electric field is radially polarized. All the other higher-order modes have nonzero longitudinal electric and magnetic field components, which are hybrid modes. For these modes in metallic nanowire, the magnetic fields along the nanowire are much small and thus they are the so-called HE modes. For the m-order modes, $2m$ nodes of the field can be found on the nanowire surface. The two m-order degenerated modes have an angle of $\pi/2m$ in the field distributions. For the HE_1 mode shown in Fig. 1(a), the electric fields point to the same direction along the x direction, but to different directions along the y direction. The two degenerated HE_1 modes correspond to dipole charge oscillations along the x or y direction vertical to the nanowire. According to the oscillation directions, the two HE_1 modes hereafter are denoted as HE_1^X and HE_1^Y.

The geometry dependent dispersion relations of the nanowire for the four lowest order modes are shown in Fig. 1(b). The TM_0 and HE_1 modes do not have cutoff as the radius of nanowire approaches to zero. With the decreasing of radius, the effective refractive index of TM_0 mode grows sharply, but that of HE_1 mode decreases. Hence, as the radius decreases, TM_0 mode becomes more confined and the mode

distribution of HE_1 spreads sharply. The increasing confinement of TM_0 mode originates from more energy penetrating into the metal region, and thus is accompanied with growing material loss as shown by the inset of Fig. 1(b). For the HE_1 mode, at a certain radius the effective refractive index is much close to that of the environment, so it is poorly confined and effectively cut off.[15] For other higher order modes, the cutoff exists and the effective refractive indexes increase with increasing nanowire radius.

2.2. Eigenmodes of pentagonal nanowire

Chemically synthesized crystallized Au and Ag nanowires have a five-fold symmetry in structure and pentagon shape in cross section. Field distributions of five lowest order modes of the pentagonal nanowire are shown in Fig. 2(a).[18] The eigenmodes of this noncircular nanowire are related to the symmetry group. They have analogy to the orbitals of the molecule with same D_{5h} group, such as the cyclopentadienyl molecule. The molecular orbitals of the cyclopentadienyl can be deduced from simple Huckel theory, and shown in Fig. 2(b) by using the conventional representation of molecular orbitals. In Fig. 2(b), the molecular orbitals are denoted by Mulliken's symbols, which can also be applied to the plasmon modes of pentagonal nanowire as shown in Fig. 2(a).

The order of the modes for pentagonal nanowire can also be classified using the number of nodes for field along the surface. The fundamental mode in pentagonal nanowire is nondegenerated, and the other higher order modes are doubly degenerated with field distributions of different shapes for the two degenerated modes, similar to the case in the cylindrical nanowire. The dispersion relations of the five lowest order modes of pentagonal nanowire are shown in Figs. 2(c) and 2(d), which show similar characteristics to those of the modes with the same order in cylindrical nanowire. The fundamental mode has an increasing effective refractive index and decreasing propagation length with reducing diameter of nanowire, while all the higher order modes show opposite tendency.

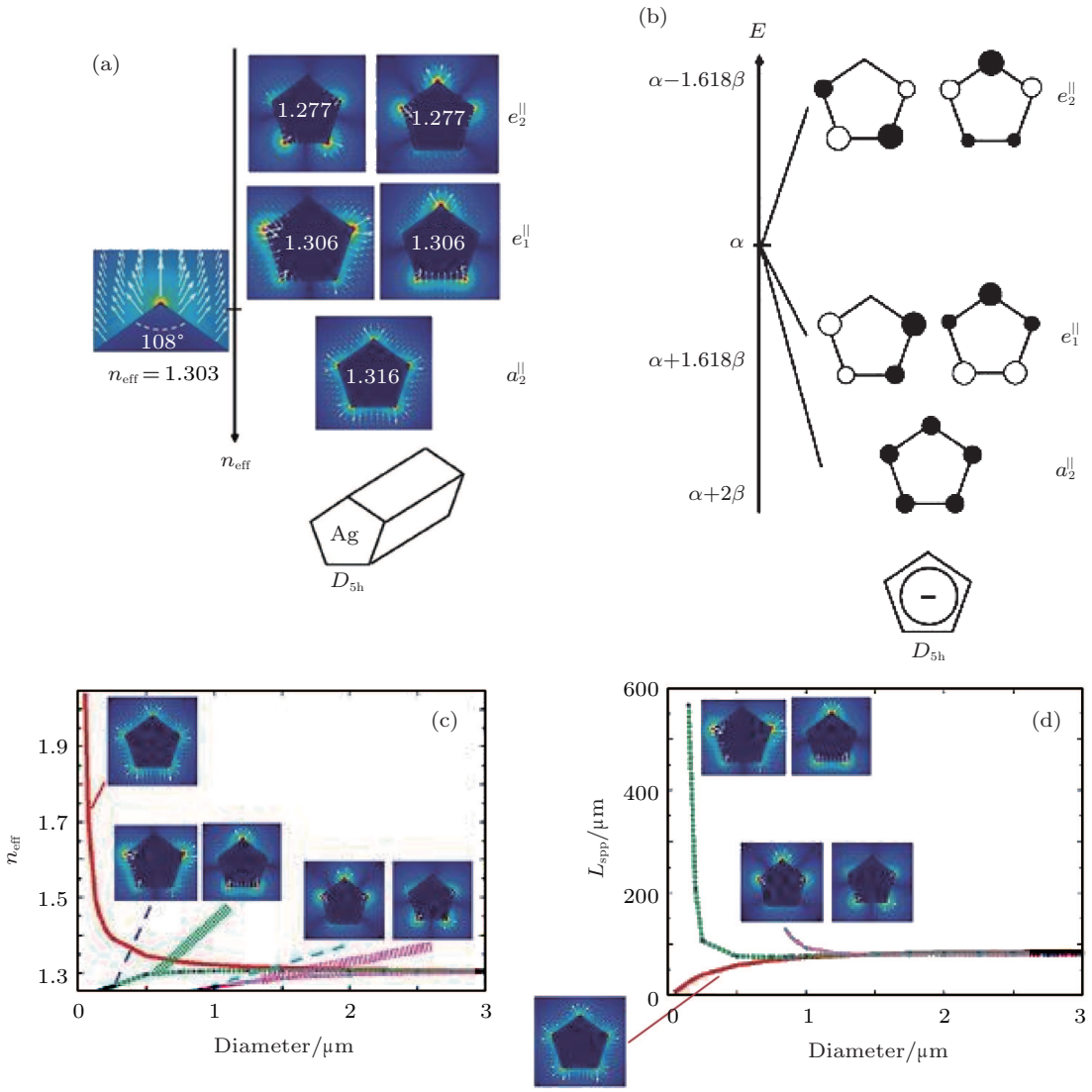

Fig. 2. (a) Field distributions of plamon modes in pentagonal silver nanowire. (b) Molecular orbitals as analogy of plasmon modes from Huckel theory. (c) Effective refractive index and (d) propagation length of plasmon modes in pentagonal silver nanowire.[18]

Unlike a cylindrical wire, a pentagonal wire contains sharp corners that can support wedge modes confined in deep sub-wavelength scale around the corner.[10,11] When the size of the wire is reduced, the wedge modes in neighboring corners start to couple to each other and reassemble into cylinder-like modes. For a significantly thin wire, the coupling between corners becomes dominant and the modes are fully like those of cylindrical wire. Therefore, the cylindrical nanowire is a good approximation for the realistic pentagonal nanowire in theoretical calculations.

2.3. Nanowire on substrate

In practical experiment, the nanowire is deposited on a substrate, so the environment is not homogeneous. This inhomogeneity will result in the change of the supported eigenmodes.[19–21] The calculated dispersion relations of three lowest order modes for nanowire with and without substrate are shown in Fig. 3(a). When a dielectric substrate is present, substrate induced symmetry breaking leads to a new set of hybridized modes, denoted as H_0, H_1, etc. The black and gray straight lines represent the dispersion relations of light in the air and glass, respectively. Only the modes with effective refractive index higher than that of the infinite environment can be bounded and propagate effectively. For individual nanowire in air, dispersion relation curves of all the three modes lie on the right side of the light line in air, so all the three modes are bounded modes. While for the hybridized modes in nanowire on the substrate, only the fundamental H_0 mode remains bounded all the time. For the two higher order H1 and H2 modes, the dispersion curve goes across the light line in glass to the left, and in this region the mode distribution is divergent in the substrate. Thus these modes are not bounded to finite region and belong to the leaky modes.[22] For these leaky modes, energy will radiate into the substrate during the propagation, leading to additional attenuation besides material loss.

The field and surface charge distributions of the modes in nanowire on substrate are shown in Figs. 3(b) and 3(c), which can be understood from the plasmon hybridization theory.[23] Different modes of nanowire in the air are orthogonal, and thus have no interactions. However, these modes may have interactions and form new hybridized modes in the nanowire-substrate system with the help of the induced charges in the substrate as shown in Fig. 3(b). The two degenerated HE_1 modes interact with the substrate and these interactions lift the degeneracy, leading to new hybridized modes. The vertical polarized HE_1 mode interacts with TM_0 mode and evolves gradually into the H_0 and H_2 modes as the substrate-mediated coupling turns stronger. Although both of the H_0 and H_2 modes come from the coupling of vertical polarized HE_1 mode and TM_0 mode, the coupling fashions are different: coupling for H_0 mode is in-phase (inducing the same polarized charges on the substrate surface), while the coupling for H_2 mode is out-of-phase (inducing opposite charges on the substrate surface). The in-phase coupling results in cancellation of the charges and field distributed on the upper surface of the nanowire for H_0 mode, while the out-of-phase coupling enhances field on the upper surface. According to the hybridization theory, the in-phase coupling leads to lower energy than the out-of-phase coupling, so the dispersion curve of H_0 mode lies below that of H_2 mode as shown in Fig. 3(a). The H_1 mode is raised from an in-phase coupling between horizontal polarized HE_1 mode and HE_2 mode and also has lower energy than H_2 mode. Figure 3(c) shows the calculated surface charges and the time-averaged power flow distributions of the three lowest order hybridized modes. The charge plots are consistent with those in Fig. 3(b), further confirming the understanding of the hybridization of different wire plasmon modes via the substrate.

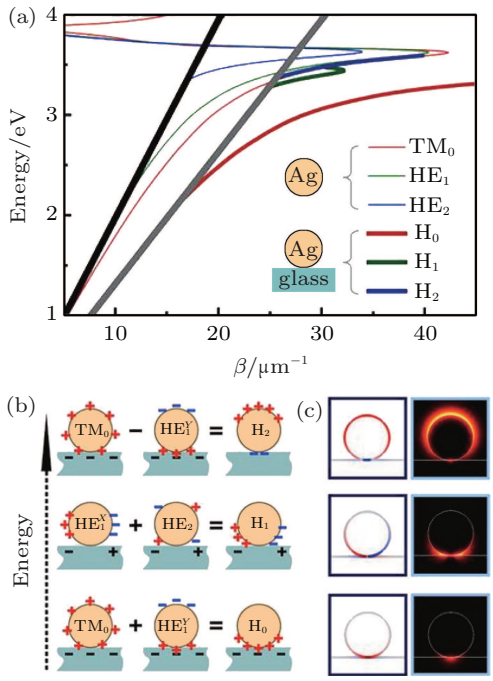

Fig. 3. (a) Dispersion relations of three lowest order modes in an Ag nanowire in air and on glass substrate (radius: 100 nm). The black and gray straight lines are light lines in air and glass, respectively. (b) Schematic of substrate induced hybridization process. (c) Calculated charge and power distributions of modes in Ag nanowire on glass substrate [20]

3. Excitation of SPPs in nanowire

3.1. Scattering method

The wave vector of SPPs in nanowire is lager than that of light waves in dielectric environment. Because of phase mismatching, the SPPs cannot be excited by light from free space directly. To excite SPPs in nanowire using light with smaller wave vector, scattering is necessary to produce wave components with larger wave vectors, which can fulfill the phase matching condition and couple into SPP modes of nanowire.

In experiments, the most commonly used method is to use a light beam focused at one terminal of the nanowire.[16,24] The excitations of different SPP modes in this method have been studied in detail in Ref. [16]. As shown in Figs. 4(a)–4(e), mode components of the excited plasmons are decided by the polarization of the incident light. The instantaneous phase of incident light φ also plays an important role when the wire is relatively thick compared with the effective incident wavelength, and the retardation effect is significant.[25] The electric fields of incident wave are aligned in the same direction on the end for $\varphi = 0$, but in opposite direction across the center of the wire for $\varphi = \pi/2$. For the polarization parallel to the nanowire, instantaneous phase of $\varphi = 0$ (Fig. 4(b)) and $\varphi = \pi/2$ (Fig. 4(c)) correspond to the most effective excitation of TM_0 and HE_1^Z modes. For the polarization vertical to the nanowire, HE_1^Y and HE_2 modes are excited for $\varphi = 0$ (Fig. 4(d)) and $\varphi = \pi/2$ (Fig. 4(e)), respectively. The excitation efficiencies of the modes are dependent on the thickness of nanowire as shown in Fig. 4(f).[26] When the polarization of the incident light is parallel to the nanowire, the coupling efficiency increases monotonically as the diameter of nanowire decreases. For much small diameter, the retardation effect is insignificant and parallel polarization mainly excite TM_0 mode. Most nanowires used for SPP propagating have relatively small diameter with their HE_2 mode being cut off. Incident light with vertical polarization will only excite HE_1 mode. As seen from the simulation result, the coupling efficiency for HE_1 mode is relatively low and reaches a maximum at about 120 nm. After coupled into the SPP modes, the light will propagate along the nanowire and emission can be observed at the other end. In the practical experiment, the nanowire is usually deposited on a substrate with the environment becoming inhomogeneous. The influence of substrate on the excitation has been studied in Ref. [27].

Scattering at other defects or discontinuous points with local symmetry breaking can also help to couple light into SPP modes of nanowire, such as the kink of bending nanowire or nanowire with an adjacent nanoparticle.[28] By direct illumination of light at the particle or the kink, the scattering can compensate for the wave vector difference and generate SPPs in the nanowire. The particle near the nanowire here essentially acts as a nanoantenna for collecting the light from free space into the nanowire. Other than nanoparticle, nanoantenna with well-designed structure can greatly enhance the in-coupling efficiency.[29] In Ref. [29], a bowtie antenna is fabricated at the input end of a silver nanowire. Compared with the nanowire without the receiving antenna, the in-coupling efficiency is enhanced by a factor of 13.6.

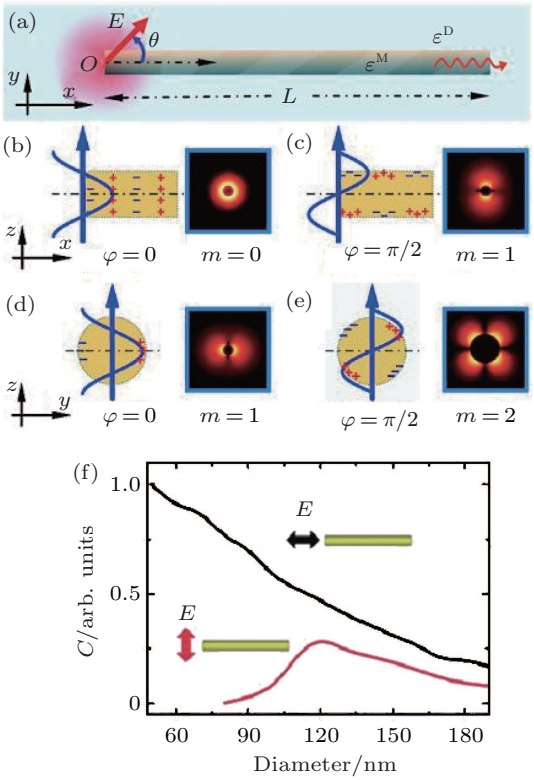

Fig. 4. Excitation of plasmon modes in metallic nanowire by direct illumination at the nanowire end. (a) Excitation scheme. (b)–(e) Plasmon mode excitation dependences on the incident polarization and instantaneous phase φ. (f) SPP excitation efficiencies in Ag nanowire for vertical and parallel polarization. Refractive index of environment is 1.518.[16,26]

3.2. Prism coupling and near field excitation

Another method to compensate for the phase mismatching is to use the evanescent wave to couple light to the nanowire from a region of higher dielectric constant. One typical example is to use the evanescent wave of total internal reflection to excite the SPPs in nanowire, namely Kretschmann setup[12,30] as shown in Fig. 5(a).[31] In this method, light can be directly coupled into the nanowire at the center of the nanowire. Under the wide field illumination, only higher order modes in the wire with the wave vector less than that of the light in the substrate can be excited directly. However, according to Subsection 2.3, these kinds of modes are in fact not bounded modes but leaky modes, and will radiate along with the propagation. The fundamental bounded mode can only be excited by scattering at nanowire ends or defects.

Phase matching condition of plasmon excitation can also be fulfilled by other near field coupling methods. The evanescent wave in the vacuum will have components with larger wave vectors at certain directions. In Fig. 5(b), the field bounded at the tip of a fiber taper has strong evanescent field outside, which may be used to excite the SPPs directly.[32,33] In this configuration, the laser light travels along the fiber to the fiber tip and couples to SPPs in the silver nanowire, which is verified by the light emission at the right end of the wire. Figure 5(c) shows the excitation of SPPs in nanowire

using ultrasmall tip of scanning near-field optical microscope (SNOM).[34] The sketch of the experimental setup is shown in the top-left of Fig. 5(c). The top-right and bottom-left insets show the optical images of SPP excitation using the SNOM tip. Exciting plasmons with the SNOM tip allows for the local excitation of SPPs in subwavelength area with the position being precisely controllable. By scanning the SNOM tip over the region marked by dash rectangle in the up-right corner in Fig. 5(c), the relation of emission intensity at the end to the position is obtained and shown in the bottom-right corner. As can be seen, the output intensity is sensitive to the position of SNOM tip, and is varied even for scanning along the direction perpendicular to the nanowire. The SNOM tip for the excitation of plasmons can be taken as a dipole point source above the nanowire.

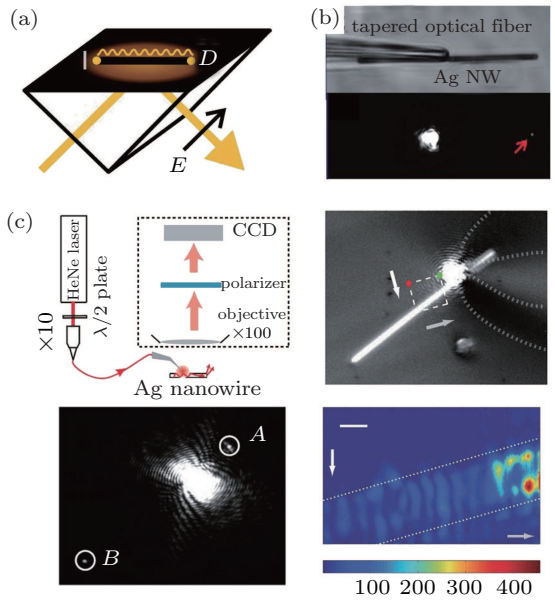

Fig. 5. Excitation of SPPs using near field. (a) Prism coupling, (b) fiber coupling and (c) coupling through SNOM probe.[31,32,34]

3.3. Electrical excitation

To generate plasmons with high localization and controllable position, apart from using SNOM tip, electrons can also be used to excite SPPs. Since the electrons have much shorter de Broglie wavelength, the localization and the position selection can be easily achieved in the scanning electron microscope (SEM) setup or by using scanning tunneling microscope (STM). Ritchie first predicted that the electron bombardment of a metal film could lead to the excitation of surface plasmons[35] and the evidences were later observed in electron energy loss spectroscopy (EELS) of aluminum films[36] and by light emission of metallic grating surfaces.[37,38] The plasmons directly excited by the fast electron beam on unstructured metal interface have been monitored through the light emission produced when SPPs are decoupled from the metal by a grating.[39] The fast electrons for the plasmon excitation have much high energy of about tens of keV or more. However, there is also a low-energy route for SPP excitation based on the inelastic electron tunneling,[40] which is the tunneling between two states of different energies. Owing to the conservation of energy, the transition of electron between the two states will be accompanied by photoemission, which can be observed in STM.[41] Advance in the field of STM has enabled the generation of photoemission on the atomic scale.[42]

The electrical excitations of plasmons in nanowires by both high energy and low-energy electrons have been discussed in the literature[43,44] which are shown in Fig. 6. The left plots in Fig. 6(a) show the plasmon excitation probability using high-energy electron of 100 keV. The result is obtained theoretically by considering the electric field induced by the incident electron and reflection of the nanowire to this field. It shows that the electron can efficiently excite $m = 0$ plasmon mode in the nanowire. Compared with the $m = 0$ mode, $m = 1$ modes are excited with smaller probability at higher energies. The plasmon-generation yield is shown with the right plots in Fig. 6(a) as obtained from the integral of the left plot over parallel wave vector $k_{//}$. This result can be obtained in experiment by EELS.

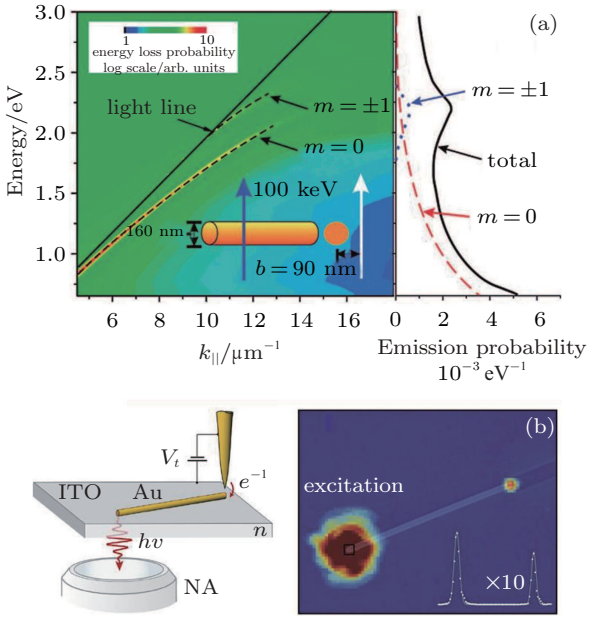

Fig. 6. (a) Electrical excitation of plasmons in silver nanowire by high energy electrons and (b) inelastic tunneling in STM.[43,44]

The electrical excitation of plasmons in silver nanowire based on inelastic electron tunneling is shown in Fig. 6(b). A bias voltage is applied between a gold nanowire and a gold tip. The inelastic electron tunneling excites a gap plasmon, which can be described by an oscillating vertical dipole. Then gap plasmons couple to plasmons propagating along the gold nanowire, and partially are scattered and converted into free-propagating photons at the other end of the nanowire. Emitted photons are collected with the objective lens and detected by a

CCD camera. Right inset in Fig. 6(b) shows the photon emission map superimposed on the SEM image.

4. Imaging SPPs in nanowire

For modes in nanowire in homogeneous environment, the field is bounded around the metal surface with larger wave vector and shorter wavelength than light in the environment. Thus, the SPPs cannot radiate into the dielectric material to form far-field observable image. For nanowire on a dielectric substrate, all the modes including leaky modes cannot radiate light into the air, so the plasmons cannot be observed from objective in the air above the substrate either. In experiments, only the SPPs converted into photons at the end of the nanowire can be detected from the air side using normal optical microscope. To detect SPPs propagating on the nanowire, special methods should be used. Some examples for typical SPP imaging methods are shown in Fig. 7. As discussed in Subsection 3.2, the SNOM can be used to excite SPPs through near field coupling. Conversely, the propagating SPPs on the nanowire can also be detected by using SNOM. Figure 7(a) shows the near field image of SPPs propagating on a silver nanowire.[31] This method utilizes the SNOM tip to convert SPPs into photons and has high spatial resolution. However, it needs particular microscopy system, and the scanning process to obtain the image may be time-consuming.

Another kind of method to obtain the image of SPPs in nanowire is to convert the near field into far-field optical signals to indirectly map the field distribution around the nanowire using far-field optical microscope.[45–47] This kind of method is optical far field method with the advantages of being easier and less expensive to implement. Figure 7(b) shows the images of SPPs in Ag nanowire by using fluorescence of quantum dots. Here the chemically synthesized silver nanowires are deposited on glass substrate and then a 30-nm thick Al_2O_3 layer is coated on the nanowire. Finally quantum dots are uniformly coated on the Al_2O_3 layer. The Al_2O_3 layer here serves as a spacer to prevent the fluorescence of the quantum dots from quenching. The fluorescence intensity is proportional to the local electric field intensity. It can be seen from the fluorescence image by exciting the quantum dots using wide field light (see ii in Fig. 7(b)) that the fluorescence is much stronger near the nanowire because the field has a very high enhancement near the wire. When SPPs are excited from the top end of the nanowire, the quantum dots are excited by the SPP field on the nanowire. The fluorescence of quantum dots reveals the near field intensity distributions of excited SPPs as shown in Fig. 7(b). Fluorescence images are recorded for the excitation of different polarizations (see iii to vi in Fig. 7(b)). These images reveal two important features: the fluorescence intensity decays exponentially along the NW, providing a direct measurement of propagation loss, and the field distribution shows a pronounced spatial modulation that depends on input polarization. This modulation is due to the interference among multiple plasmon modes.

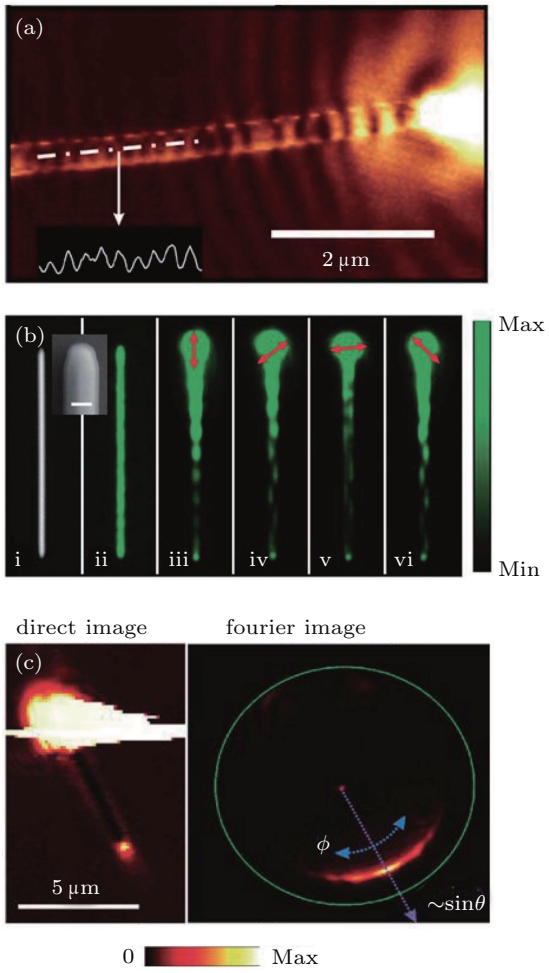

Fig. 7. (a) Direct imaging of SPPs in nanowire using SNOM. (b) Quantum dots-based fluorescence imaging of SPPs in nanowire. (c) Optical image from leaky radiation in substrate and its Fourier image.[31,45,48]

For nanowire on a dielectric substrate, when the mode is leaky, it can radiate electromagnetic wave into the substrate and this signal can be collected for the optical imaging of SPPs in nanowire. Figure 7(c) shows the optical imaging from the leaky radiation in the substrate.[48] A nanowire was deposited on glass substrate and the SPPs in the nanowire were generated using a focused light beam at one end of the wire. The leaky radiation into the glass substrate was collected using a high numerical aperture oil-immersed objective. As can be seen from the leaky radiation image at the left of Fig. 7(c), apart from the emission scattered at the end of the wire, there is light emitted from the whole nanowire. The direction distribution of the radiation can be obtained from the Fourier image at the back focal plane of the objective. It can be seen from the Fourier image at the right of Fig. 7(c) that the radiation is highly unidirectional, which makes the nanowire a nanoantenna with good directionality.

5. Propagation of SPPs in nanowire

In Section 2, the basic plasmon eigenmodes of nanowire have been discussed. In general situation, the guiding plasmons are superposition of these modes and show a peculiar spiral propagating route on the nanowire.[16] By illuminating the end of the nanowire with a beam polarized at an angle with respect to the nanowire, e.g., 45° as shown in Fig. 8(a), the TM_0 mode and two HE_1 modes are simultaneously generated. As stated in Subsection 3.1, the two excited HE_1 modes have a phase difference of $\pi/2$, and their superposition will bring angular momentum. In this excitation scheme, the TM_0 mode is also excited simultaneously. The superposition of two HE_1 modes is of cylindrical symmetry in amplitude with phase decreasing with rotation angle, and the TM_0 mode also has a cylindrically symmetrical amplitude distribution but with a uniform phase. Superposition of the three modes will have a maximum and a minimum on the opposite side of the nanowire. Along with the propagation, the maximum point moves around the nanowire surface, showing a spiral propagating route, which can be seen in Figs. 8(a) and 8(b). The spiral propagation is chiral, whose chirality is determined by the excitation polarization. The period of the chiral propagation is determined by the difference in phase accumulating along with the propagation: $\text{Period} = \lambda/\text{Re}(n_0 - n_1)$, where n_0 and n_1 are the effect refractive indexes of TM_0 and HE_1 modes, which depend on the diameter of nanowire, and λ is the wavelength of the excitation light. The period increases with the increase of the nanowire radius as shown in Fig. 8(c). For the nanowires on substrate, the SPPs propagate as superposition of the new hybridized modes and the spiral propagation route is disturbed, turning into zigzag shape as shown in Fig. 7(b).[45]

The SPPs propagating in the nanowire may suffer bending loss and material loss. For practical applications, the bending of wire is needed to construct plasmonic circuit. At the bending, the plasmons will suffer bending losses and radiate power into outer environment. The bending loss is related to the radius of the bending, which has been studied experimentally.[32] The material loss of nanowire[49] is inevitable, which originates from the ohmic heat producing of metal. Increasing the confinement of SPPs, as an example, by increasing the permittivity of the environment, will result in more energy penetrating into the metal, thus suffering higher ohmic loss. Therefore, introducing substrate to support the nanowire will increase confinement and material loss.[27] Meanwhile, the substrate will also change the bounded plasmon modes into leaky modes, and bring about leaky loss. The propagation loss is a key problem for plasmonic circuits, which may be solved by introducing gain materials[50–52] and integrating with other low-loss dielectric waveguides.[53]

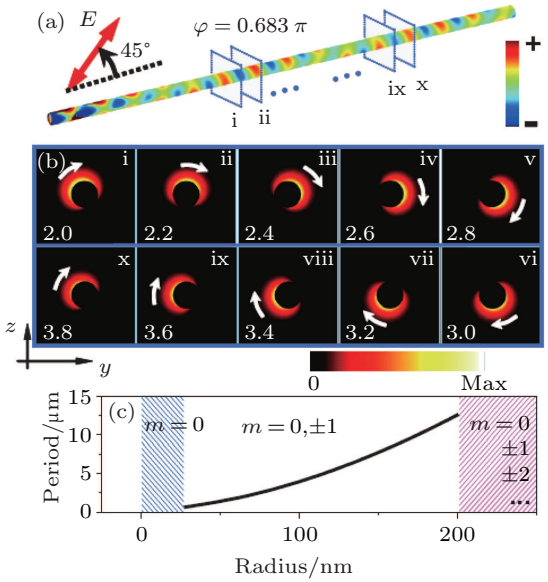

Fig. 8. (a) Surface charge density plot on an Ag nanowire of radius 60 nm. (b) Time-averaged power flow in the y–z plane at different positions along the nanowire, where x is from 2.0 to 3.8 μm (i–x) in steps of 0.2 μm, indicated by the blue frames in panel (a). The white arrows highlight the rotation of electromagnetic energy as a function of position along metal nanowire. (c) Periods of the plasmon helix as a function of nanowire radius. The blue region denotes the single mode-dominant regime, and the magenta region denotes the multimode regime.[16]

6. Emission of SPPs in nanowire

The conversion of SPPs into photons at the ends of the nanowire is the reverse process of SPP excitation by direct illumination at the end of nanowire. For the reciprocity, this emission happens with the same efficiency as the SPP excitation. Metallic nanowires behave like nanoantennas to modulate the emission of SPPs in the nanowires.[26,48,54,55] The emission at the end of nanowire can be taken as superposition of the emissions from different modes mentioned in Section 2. Figure 9(a) shows the emission characteristics of the modes at the end of nanowire embedded in homogeneous dielectric environment. As can be seen, the emission fields maintain the polarization symmetry of the modes propagating in the nanowire. For the TM_0 mode, the electric field direction at each point is along the radial direction of the cylindrical nanowire. The emission of TM_0 mode is also radially polarized with axial symmetry. For this vector field, singular point exists along the axis of the nanowire where the polarization is undetermined, resulting in the zero amplitude there. As shown in Fig. 9(a), the distribution of the TM_0 mode emission is angular, and the maximum intensity is along the direction with an inclination of about 30° from the axial direction of nanowire. For the HE_1 mode, the emission is linearly polarized. The maximum intensity is along the axial direction with a small spreading angle of 15°. Therefore, the HE_1 mode has concentrated emission power and directionality, which can be used for designing high-gain nanoantennas. The emission features of the plasmon modes can be intuitively understood as results of the dipole

emission at the end tip of the nanowire.

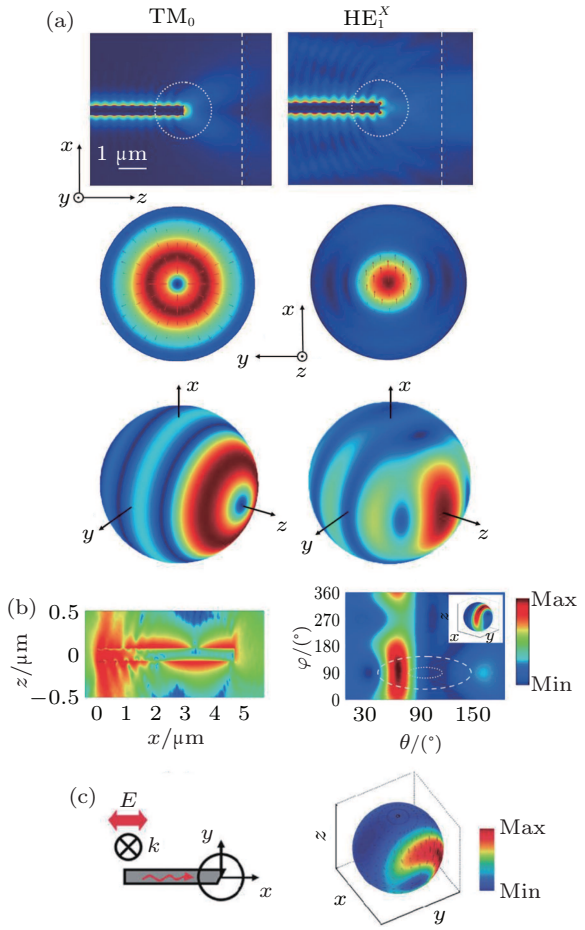

Fig. 9. (a) Emission characteristics of TM_0 and HE_1 mode in nanowire Top row: electric field amplitudes on cut plane across the axis of the wire; middle row: electric field amplitudes on cut plane 2 μm away from the output terminus marked by dash line in the top row; bottom row: the far field angular emission distributions transformed from spheres marked by the dot circles in top row. (b) Directional emission of nanowire excited by illuminating one end to generate both TM_0 and HE_1 modes. (c) Effect of nanowire end geometry on the emission.[26,55]

For excitation of SPPs by illuminating the end of the nanowire, both TM_0 mode and HE_1 mode are generated. The emission from the nanowire end is the superposition of the emissions from these two modes. The result of this superposition leads to the violation of emission symmetry and the redirection of the emission power as shown in Fig. 9(b).[55] The left panel shows the intensity distribution of Poynting vectors of a nanowire excited by direct illumination. It can be seen that the distribution of SPPs on the wire are nonsymmetrical and the emission at the end is at an angle with respect to the wire axis. The directional emission is further confirmed by far-field angular distribution shown in the right panel. The emission is sensitive to the geometrical shape of the nanowire end as it determines the relative intensity of two plasmon modes.[26] As shown in Fig. 9(c), a wire with a flat incident end and a 60° side-cut emission end is excited by parallel polarized light. Here, only the TM_0 mode is excited, but the emission intensity is asymmetric because of the asymmetric shape of the emission nanowire end.

7. Nanowire based photonic devices

7.1. Quarter-wave plate

Quarter-wave plate is one of the most basic optical elements used in optical experiments, which can change the polarization state of light traveling through it from linear polarization to circular polarization. The traditional wave-plate is constructed using birefringent materials with different refractive indexes for two orthogonal polarizations, which introduces a phase difference of $\pi/2$ for proper plate thickness. At the nanoscale, several kinds of super thin quarter wave plates have been realized by metasurfaces.[56,57] It has also been demonstrated that metallic nanowires can be used as quarter-wave plates.[16]

By illuminating one end of nanowire with a beam of light linearly polarized at an angle with respect to the wire, the excited two $m = 1$ modes have a phase difference of $\pi/2$. Although the superposition fields of the two modes near the wire are linearly polarized at each point, the emission will show circular polarization. Considering the direction along the axis of the nanowire, the emissions of the two modes reach the maxima with a phase difference of $\pi/2$, yielding a circular polarization. In the excitation scheme, the TM_0 mode is also generated and influences the emission symmetry. Figure 10 shows the circular polarization degree and figure of merit (FOM) of the field in the vertical plane beyond the output end of the nanowire. For nanowire aligned along the z direction, the circular polarization degree C and figure of merit (FOM) f are defined here as

$$C = \frac{2\langle E_y(t)E_z(t)\sin(\delta_y - \delta_z)\rangle}{\langle E_x^2(t)\rangle + \langle E_y^2(t)\rangle + \langle E_z^2(t)\rangle}, \quad f = \frac{|E(\vec{r})|^2}{|E_0(0)|^2} \times C^2, \quad (2)$$

where $E_0(0)$ is the incident electric field at the origin, $\delta_y - \delta_z$ is the phase difference between the two transverse electric field components E_y and E_z. The results in Fig. 10 confirm the high degree of circular polarization of the outgoing optical wave.

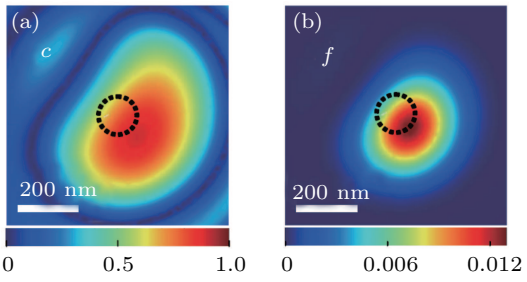

Fig. 10. (a) Circular polarization degree C and (b) figure of merit f in a vertical plane 200 nm beyond the output end of a nanowire excited by linearly polarized light. The black dot circles denote the cross section of the nanowire.[16]

7.2. Fabry–Pérot resonator

The plasmon modes in the nanowire have higher effective refractive indexes than the index that the light in free space has. The light transmitted from the free space into the nanowire, or in the reverse process will have part of power reflected, just like the light incident on an interface between two dielectric materials. From this point of view, a nanowire with a finite length will resemble the Fabry–Pérot (F–P) cavity formed by two parallel interfaces.[31]

SPPs in single-crystalline nanowires can be excited using total internal reflection in prism as mentioned in Subsection 3.2. White light from halogen lamp is used for the excitation. Scattered light spectra from both input and output ends of nanowires show clear line shapes of F–P resonator modes as shown in Fig. 11(a). Signal minima in the spectrum from the input end correspond to maxima from the distal wire end, which confirms that the spectra are raised from F–P resonance in the nanowire, just like resonance in two parallel placed mirrors. By assigning the plasmon resonance orders, which can be determined by the SNOM image of the nanowire SPPs, to the individual signal peaks in the spectrum, the dispersion relation can be deduced as shown in Fig. 11(b). The deduced dispersion relation of the nanowire SPPs lies below both light lines in air and in the glass substrate, so this signal corresponds to the fundamental bonded SPP mode of the nanowire on substrate.

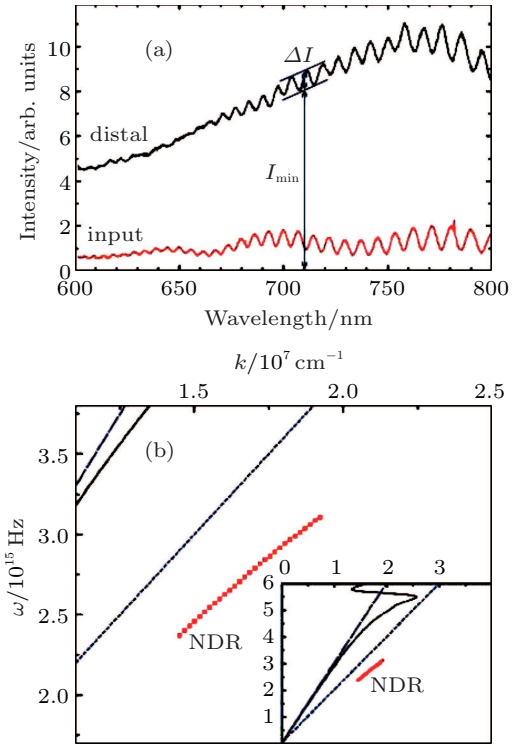

Fig. 11. (a) Spectra of scattered light from the input and distal end of a silver nanowire of length 18.6 μm and diameter 120 nm (b) Dispersion relation of the nanowire SPPs (NDR) deduced from panel (a). The solid black line corresponds to the SPPs at a flat silver-air interface. The long- and short-dashed curves correspond to the light lines in air and the glass substrate, respectively.[31]

7.3. Router

In the networks for nanophotonic circuits, plasmonic routers are needed to control the transmission of SPPs. It was demonstrated that a branched nanowire structure shown in Fig. 12(a) can be used as a plasmonic router.[58] In the branched structure, there are three ports, denoted as 1, 2, and 3. After exciting the SPPs in nanowire at port 1, the SPPs can propagate to both nanowire branches and finally radiate at port 2 and port 3. The emissions from the two ports are recorded and their dependences on the polarization of the incident light are shown in Fig. 12(b). For excitation under laser light of either 632.8 nm or 785 nm, the emissions on both output terminals have maximum intensities for certain polarizations. Thus, the plasmon energy can be controllably routed to port 2 or 3 by manipulating the incident polarization. It can also be seen that the polarization dependences for the two wavelengths are different. Under bicolor illumination of these two wavelengths with the same polarization as shown in Fig. 12(c), the light components of different colors are separated and directed to different ends. This is just as a de-multiplexer for the wavelength division multiplexing (WDM). The routing function realized in the nanowire originates from the nonuniform near field distribution of the SPPs. The polarization and the wavelength of the incident light can influence the field distribution at the node of the branch, and finally determine the flow direction of plasmon energy.[21,45] Moreover, the active control of the power flow routes can be realized by tuning the refractive index of the environment or the dielectric coatings on the nanowires.[21]

7.4. Logic gates

The electronic integrated circuit is based on a huge number of basic logic gates. To build nanophotonic integrated circuit, the realization of nanophotonic logic gates is of fundamental significance. By utilizing the coherence of SPP signals, Boolean logic gates are realized in nanowire-based structures.[45,59] Interference between two SPP signals propagating along silver nanowire can be achieved in the branch nanowire structure as shown in Fig. 13(a). The two terminals for launching the SPP signals are denoted as I1 and I2, and the third terminal for output signals is denoted as O. By illuminating two coherent laser beams with tunable phase at the two input terminals I1 and I2, two SPP signals are launched into the long nanowire. By tuning the phase difference between the two input beams, the intensity of the output signal is strongly modulated as shown in Fig. 13(b), indicating that the two SPP signals are highly coherent. The optical scattering images and corresponding quantum dot fluorescence images for the constructive and destructive interference of the two plasmon beams are shown in Fig. 13(c). As can be seen, the SPP interference can modulate both the output intensity at terminal

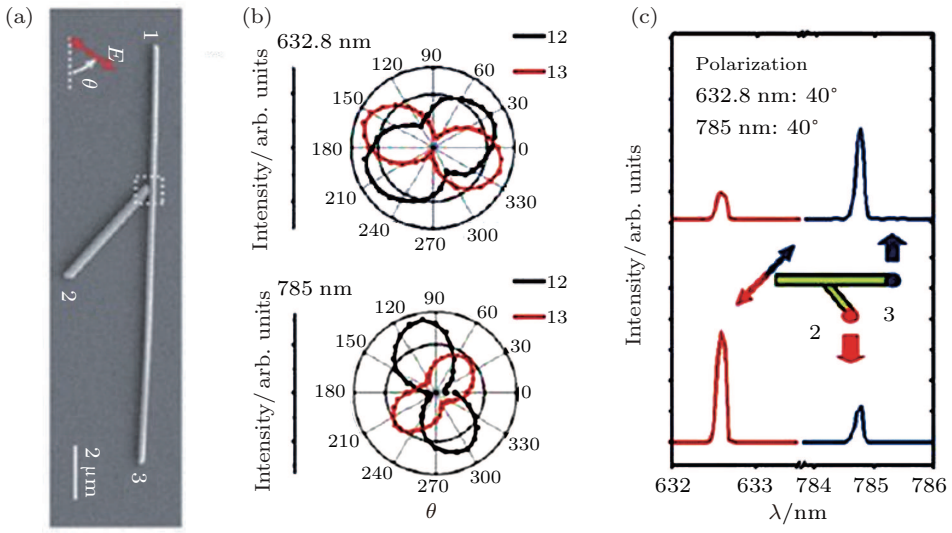

Fig. 12. Branched nanowire structure as a router for SPPs. (a) The SEM image of a branched silver nanowire structure. θ is the angle of the incident polarization. (b) Emission intensity from nanowire port 2 (black) and 3 (red) as a function of incident polarization angle for excitation with wavelengths of 632.8 nm and 785 nm. (c) The spectra of output light from ports 2 and 3 for bicolor excitation with wavelengths of 632.8 nm and 785 nm.[58]

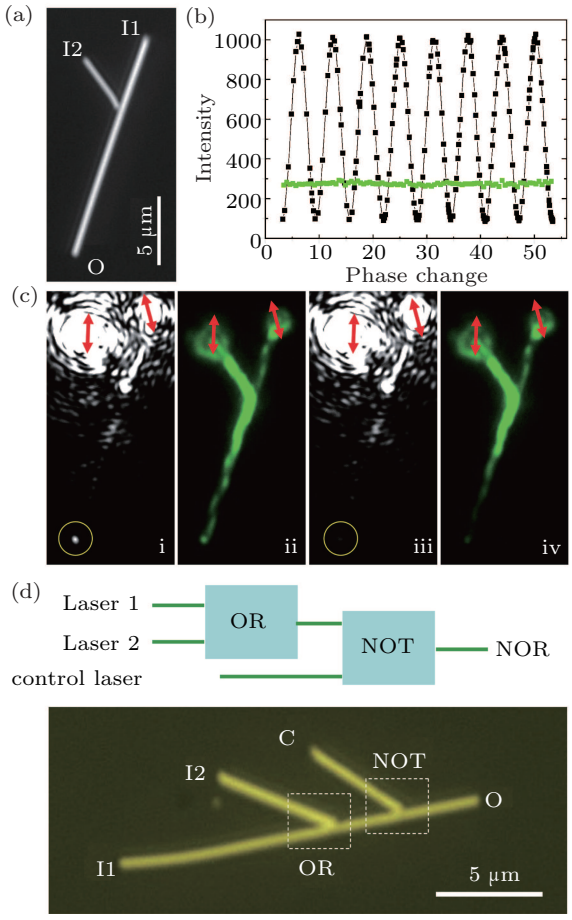

Fig. 13. (a) Optical image of branch nanowire as optical logic gate. (b) Emission intensity from port O as a function of phase delay between two incident beams. (c) (i, iii) Scattering images for constructive and destructive interference of two incident beams. (ii, iv) Quantum dot fluorescence images corresponding to (i) and (iii). The Al_2O_3 thickness is 30 nm. Red arrows indicate the polarizations of the two incident beams. (d) Schematic illustration of a NOR logic gate, built by cascaded OR and NOT gates (top) and optical image of designed Ag nanowire-based structure (bottom).[45,59]

O and the near field distribution along the nanowire. The SPP interference makes the branched nanowire structure work as a plasmonic Boolean logic gate. Proper threshold values can be defined for output state as "1", and the intensity lower than the threshold corresponds to the output state "0". Considering the intensity values shown in Fig. 13(b), for destructive interference, a defined threshold value of 200 makes the structure accomplish the logic function of XOR gate. For constructive interference, a defined threshold value of 600 or 200 makes the branch nanowire an AND or OR gate. By taking one input as an invariant control signal, the output signal is opposite to the other input signal for destructive interference and a threshold value of 200, making the structure a NOT logic gate.

To perform complicated computing, the fundamental logic gates must be cascaded. The nanowire based logic gates have cascadability, making them promising elements for future optical computing. One example for the cascaded logic function is shown in Fig. 13(d). The structure is constructed by cascading two branch nanowire logic gates in Fig. 13(a). In this structure, the two branches are separately working as NOT and OR gates. The experiments demonstrate that the output result corresponds to a NOR gate cascaded by the two gates.

8. Conclusions and outlook

In this review, we present the recent research results on the basic properties of metallic nanowire waveguides and nanowire-based photonic devices. Metallic nanowire is basically multimode waveguide. The plasmon modes in ideal nanowire and practical nanowires used in experiments are analyzed. Nanowire plasmons can be excited by optical or electrical methods, and detected by near-field or far-field techniques. Because of the multimode characteristic, the plasmon propa-

gation and emission in the nanowire have many unique properties, thereby making it much flexible to design plasmonic devices. The nanowire-based photonic devices make the light signal control at subwavelength scale, and are important elements for constructing nanophotonic integrated circuits.

As SPPs can be strongly influenced by the dielectric surroundings, the properties of nanowire SPPs can be tailored by controlling the dielectric constant of the environmental medium. Therefore, composite structures of metallic nanowires and materials with especial properties will show peculiar performances unattainable in bare nanowires. Active materials can be incorporated to compensate for the propagation loss of SPPs, which is important for avoiding the signal distortion during transmission. The development of advanced nanowire manipulation techniques will definitely be conducive to the construction of nanowire networks and complex structures. To make high-performance nanophotonic devices and circuits for practical applications, the interconnection of plasmonic devices with photonic and electronic devices can be critical, which needs further efforts to investigate the hybridization of the different devices.

References

[1] Kok P, Munro W J, Nemoto K, Ralph T C, Jonathan D P and Milburn G J 2007 *Rev. Mod. Phys.* **79** 135
[2] Xu H X, Aizpurua J, Käll M and Apell P 2000 *Phys. Rev. E* **62** 4318
[3] Tong L M, Wei H, Zhang S P, Li Z P and Xu H X 2013 *Phys. Chem. Chem. Phys.* **15** 4100
[4] Maier S 2007 *Plasmonics: Fundamentals and Applications* (Berlin: Springer)
[5] Steinberger B, Hohenau A, Ditlbacher H, Stepanov A L, Drezet A, Aussenegg F R, Leitner A and Krenn J R 2006 *Appl. Phys. Lett.* **88** 094104
[6] Holmgaard T and Bozhevolnyi S 2007 *Phys. Rev. B* **75** 245405
[7] Veronis G and Fan S 2005 *Opt. Lett.* **30** 3359
[8] Pile D F and Gramotnev D K 2004 *Opt. Lett.* **29** 1069
[9] Bozhevolnyi S I, Volkov V S, Devaux E and Ebbesen T W 2005 *Phys. Rev. Lett.* **95** 046802
[10] Pile D F P, Ogawa T, Gramotnev D K, Okamoto T, Haraguchi M, Fukui M and Matsuo S 2005 *Appl. Phys. Lett.* **87** 061106
[11] Moreno E, Rodrigo S G, Bozhevolnyi S I, Martín-Moreno L and García-Vidal F J 2008 *Phys. Rev. Lett.* **100** 023901
[12] Dickson R M and Lyon L A 2000 *J. Phys. Chem. B* **104** 6095
[13] Sun Y G and Xia Y N 2002 *Adv. Mater.* **14** 833
[14] Jackson J D 1999 *Classical Electrodynamics* (New York: Wiley)
[15] Chang D E, Sϕrensen A S, Hemmer P R and Lukin M D 2007 *Phys. Rev. B* **76** 035420
[16] Zhang S P, Wei H, Bao K, Hakanson U, Halas N J, Nordlander P and Xu H X 2011 *Phys. Rev. Lett.* **107** 096801
[17] Marcuse D 1991 *Theory of Dielectric Optical Waveguides* (San Diego: Academic Press)
[18] Song M X, Bouhelier A, Bramant P, Sharma J, Dujardin E, Zhang D G and Colas-des-Francs G 2011 *ACS Nano.* **5** 5874
[19] Zou C L, Sun F W, Xiao Y F, Dong C H, Chen X D, Cui J M, Gong Q, Han Z F and Guo G C 2010 *Appl. Phys. Lett.* **97** 183102
[20] Zhang S P and Xu H X 2012 *ACS Nano* 6 8128
[21] Wei H, Zhang S P, Tian X R and Xu H X 2013 *Proc. Natl. Acad. Sci.* **110** 4494
[22] Hu J and Menyuk C R 2009 *Adv. Opt. Photon.* **1** 58
[23] Prodan E, Radloff C, Halas N J and Nordlander P A 2003 *Science* **302** 419
[24] Sanders A W, Routenberg D A, Wiley B J, Xia Y N, Dufresne E R and Reed M A 2006 *Nano Lett.* **6** 1822
[25] Hao F, Larsson E M, Ali T A, Sutherland D S and Nordlander P 2008 *Chem. Phys. Lett.* **458** 262
[26] Li Z P, Bao K, Fang Y R, Huang Y Z, Nordlander P and Xu H X 2010 *Nano Lett.* **10** 1831
[27] Li Z P, Bao K, Fang Y R, Guan Z Q, Halas N J, Nordlander P and Xu H X 2010 *Phys. Rev. B* **82** 241402
[28] Knight M W, Grady N K, Bardhan R, Hao F, Nordlander P and Halas N J 2007 *Nano Lett.* **7** 2346
[29] Fang Z Y, Fan L R, Lin C F, Zhang D, Meixner A J and Zhu X 2011 *Nano Lett.* **11** 1676
[30] Raether H 1988 *Surface Plasmons on Smooth and Rough Surfaces and on Gratings* (New York: Springer Verlag)
[31] Ditlbacher H, Hohenau A, Wagner D, Kreibig U, Rogers M, Hofer F, Aussenegg F R and Krenn J R 2005 *Phys. Rev. Lett.* **95** 257403
[32] Wang W H, Yang Q, Fan F R, Xu H X and Wang Z L 2011 *Nano Lett.* **11** 1603
[33] Li Q, Wang S S, Chen Y T, Yan M, Tong L M and Qiu M 2011 *IEEE J. Sel. Top in Quantum Electron* **17** 1107
[34] Liu N, Li Z P and Xu H X 2012 *Small* **8** 2641
[35] Ritchie R H 1957 *Phys. Rev.* **106** 874
[36] Powell C J and Swan J B 1959 *Phys. Rev.* **115** 869
[37] Teng Y and Stern E 1967 *Phys. Rev. Lett.* **19** 511
[38] Heitmann D 1977 *J. Phys. C: Solid State Phys.* **10** 397
[39] Bashevoy M V, Jonsson F, Krasavin A V, Zheludev N I, Chen Y and Stockman M I 2006 *Nano Lett.* **6** 1113
[40] Lambe J and McCarthy S L 1976 *Phys. Rev. Lett.* **37** 923
[41] Gimzewski J K, Reihl B, Coombs J H and Schlittler R R 1988 *Z. Phys. B* **72** 497
[42] Aizpurua J, Hoffmann G, Apell S P and Berndt R 2002 *Phys. Rev. Lett.* **89** 156803
[43] Cai W, Sainidou R, Xu J, Polman A and García de Abajo F J 2009 *Nano Lett.* **9** 1176
[44] Bharadwaj P, Bouhelier A and Novotny L 2011 *Phys. Rev. Lett.* **106** 226802
[45] Wei H, Li Z P, Tian X R, Wang Z X, Cong F Z, Liu N, Zhang S P, Nordlander P, Halas N J and Xu H X 2011 *Nano Lett.* **11** 471
[46] Wild B, Cao L, Sun Y, Khanal B P, Zubarev E R, Gray S K, Scherer N F and Pelton M 2012 *ACS Nano.* **6** 472
[47] Solis D, Chang W S, Khanal B P, Bao K, Nordlander P, Zubarev E R and Link S 2010 *Nano Lett.* **10** 3482
[48] Shegai T, Miljkovic V D, Bao K, Xu H X, Nordlander P, Johansson P and Käll M 2011 *Nano Lett.* **11** 706
[49] Ma Y G, Li X Y, Yu H K, Tong L M, Gu Y and Gong Q H 2010 *Opt. Lett.* **35** 1160
[50] Bergman D J and Stockman M I 2003 *Phys. Rev. Lett.* **90** 027402
[51] De Leon I and Berini P 2010 *Nat. Photon.* **4** 382
[52] Liu N, Wei H, Li J, Wang Z X, Tian X R, Pan A L and Xu H X 2013 *Sci. Rep.* **3** 1967
[53] Guo X, Qiu M, Bao J M, Wiley B J, Yang Q, Zhang X N, Ma Y G, Yu H K and Tong L M 2009 *Nano Lett.* **9** 4515
[54] Dorfmuller J, Vogelgesang R, Khunsin W, Rockstuhl C, Etrich C and Kern K 2010 *Nano Lett.* **10** 3596
[55] Li Z P, Hao F, Huang Y Z, Fang Y R, Nordlander P and Xu H X 2009 *Nano Lett.* **9** 4383
[56] Drezet A, Genet C and Ebbesen T W 2008 *Phys. Rev. Lett.* **101** 043902
[57] Yu N, Aieta F, Genevet P, Kats M A, Gaburro Z and Capasso F 2012 *Nano Lett.* **12** 6328
[58] Fang Y R, Li Z P, Huang Y Z, Zhang S P, Nordlander P, Halas N J and Xu H X 2010 *Nano Lett.* **10** 1950
[59] Wei H, Wang Z X, Tian X R, Käll M and Xu H X 2011 *Nat. Commun.* **2** 387